

Supplement of Atmos. Chem. Phys., 19, 7883–7896, 2019
<https://doi.org/10.5194/acp-19-7883-2019-supplement>
© Author(s) 2019. This work is distributed under
the Creative Commons Attribution 4.0 License.



Supplement of

Long-term aerosol optical hygroscopicity study at the ACTRIS SIRTA observatory: synergy between ceilometer and in situ measurements

Andrés Esteban Bedoya-Velá et al.

Correspondence to: Andrés Esteban Bedoya Velásquez (aebedoyav@correo.ugr.es)

The copyright of individual parts of the supplement might differ from the CC BY 4.0 License.

1 Effect of beta-attenuated water vapor correction on calculated $f_\beta(RH)$ and γ parameter

The β^{att} signal presents a dependency on water vapor absorption as shown in Sec. 3.1 (Eq.8), associated with the wavelength emission. This dependency may cause direct effects over calculations retrieved by using β^{att} . Here, we present the correction applied to β^{att} and the effects on $f_\beta(RH)$ and γ calculations. Figure S1 (left-panels) represents the temporal-evolution of β^{att} , beta attenuated water vapor corrected (β_{wv}^{att}) signals over 3 h time-window, together with the temporal-evolution of q . Figure S1 (right-panels) shows the biases for beta ($bias_\beta$) and Δ_q obtained.

The quantifications are performed by means of the bias $_\beta$ ($\beta^{att} - \beta_{wv}^{att}$) and Δ_q ($q(t) - q(t_d)$) calculations. Fig. S1ac presents two cases (case 1 and case 2) with low absolute-differences in q , which produces slight changes in β_{wv}^{att} signal respect to β^{att} . On the other hand, Fig. S1eg (case 3 and case 4) show that high absolute-differences in q are linked to high changes on β_{wv}^{att} . The right side of the panel (Fig. 1Sbd, case 1 and case 2), presents the bias quantification, showing that low bias $_\beta$ are associated with low Δ_q and, on the contrary, Fig. 1Sfh (case 3 and case 4), show that increases in Δ_q makes that bias $_\beta$ becomes higher. This analysis leads us to conclude that no-water vapor correction will produce an overestimation of the total β signal, being Δ_q the parameter that rules the β correction. From now, we will use β instead of β^{att} for simplicity.

To see the effect of β_{wv}^{att} on $f_\beta(RH)$, we applied the Hänel parameterization (Eq. 7, Sec. 3.1 of the manuscript) to the same 4 cases studied above. Figure S2 presents the $f_\beta(RH)$ and the enhancement factor water vapor corrected, $f_{\beta_{wv}^{att}}(RH)$. The results reinforce those obtained above (Fig S1), where low/high changes in Δ_q are linked with low/high bias $_\beta$ and, on this way, this would affect $f_\beta(RH)$ calculation. Additionally, the water vapor correction tends to decrease γ (β_{wv}^{att} is lower than β). Therefore, cases with lower bias $_\beta$ and Δ_q (case 1 and case 2), exhibits lower $bias_\gamma$ (0.02 and 0.05, respectively), meanwhile on case 3 and case 4 instead bias $_\beta$ increase, the $bias_\gamma$ becomes higher (0.11 and 0.09, respectively).

Once we applied the phase 2 of the methodology (Sec. 5), we obtain 94 hygroscopic potential cases for 3h time-window (Fig. S3a), 9 cases for 4h time-window (Fig. S3a) and 4 cases for 5h time-window (Fig. S3a), resulting in a total of 107 cases. To establish a bias error for this hygroscopic study, we have calculated the median of the bias $_\beta$ and Δ_q , highlighting two main aspects: (i) The median bias $_\beta$ follows the median Δ_q variability, remarking their dependency. This fact is well seen from the scatter plot (Fig. 3Sb), where these variables show a positive correlation, however the correlation coefficient is not too high ($R^2= 0.61$), mainly because the data dispersion increases for bias $_\beta > 1.5 \cdot 10^{-7} \text{ m}^{-1} \cdot \text{sr}^{-1}$ and $\Delta_q > 3.0 \text{ g/m}^3$; (ii) The mean bias error calculated for β_{wv}^{att} over the 107 potential cases evaluated is lower than $2.5 \cdot 10^{-7} \text{ m}^{-1} \cdot \text{sr}^{-1}$ and the mean Δ_q is lower than 5.5 g/m^3 .

Fig. S4 quantifies the effect of the β_{wv}^{att} over $f_{\beta}(RH)$ and γ hygroscopic properties, by means of the median bias $_{f_{\beta}(RH)}$ ($f_{\beta}(RH) - f_{\beta_{wv}^{att}}(RH)$) and the bias γ ($\gamma_{\beta^{att}} - \gamma_{\beta_{wv}^{att}}$). Figure S4 reveals the no-correlation between bias $_{\beta}$ and bias $_{f_{\beta}(RH)}$. However, combining the results from Fig. S3 and Fig. S4, it is possible to establish that bias $_{\beta} > 1 \text{ m}^{-1} \cdot \text{sr}^{-1}$ would cause an increment of bias $_{f_{\beta}(RH)}$ above 0.2, increasing the error on $f_{\beta}(RH)$. Finally, it was obtained that bias $_{f_{\beta}(RH)}$ and bias γ for the whole study were lower than 0.3.

2 Results

2.1 Methodology applied to eight aerosol hygroscopic growth cases

The 8 hygroscopic growth cases reported in this study (Table 1, Sec. 5.2) were found at daytime in the early morning, with RH_{ref} around 50 % and the maximum RH reached was up to 90% over 3h time-window. For cases 1, 2, 4, 5, 6 and 7 the perceptual composition was dominated by OA with values up to 50 %, except on case 7 where OA decreased up to 38%. The BC concentration was relatively low almost for all cases found (close to 6 %). The concentration of inorganic compounds were dominated by SO_4^{2-} (lower than 21 %) and NH_4^+ (lower than 19 %), however NO_3^- reached values of 21% on case 6. The air masses that come mainly from W-NW direction are related to case 1 ($\Delta u=3.6 \text{ m/s W}$), case 2 ($\Delta u=23.0 \text{ m/s NW}$) and case 6 ($\Delta u=4.4 \text{ m/s W}$), with speed variability up to 14.2 %, 20.7 % and 18.5 %, respectively; and the air masses that coming from W-SW direction at low wind direction variability are associated with case 4 ($\Delta u=2.7 \text{ m/s W}$), case 5 ($\Delta u=2.4 \text{ m/s SW}$), and case 7 ($\Delta u=1.7 \text{ m/s SW}$), and wind speed variability about 15.4 m/s, 20.4 m/s and 10.9 m/s, respectively. All these cases fulfilled the threshold established for $\frac{\Delta f_{PM1}(RH)}{\Delta f_{\beta}(RH)} < 0.5$ indicating that increases/decreases in $f_{\beta}(RH)$ are not related with advected aerosol into the atmospheric volume studied. The Hanel parameterization is calculated for both $f_{\beta}(RH)$ and $f_{PM1}(RH)$ (see panel Fig. S4 to S9 b.). The hygroscopicity properties of the 6 cases presented here were evaluated and compared against literature in the Sec. 5.2 of the article.

Figures

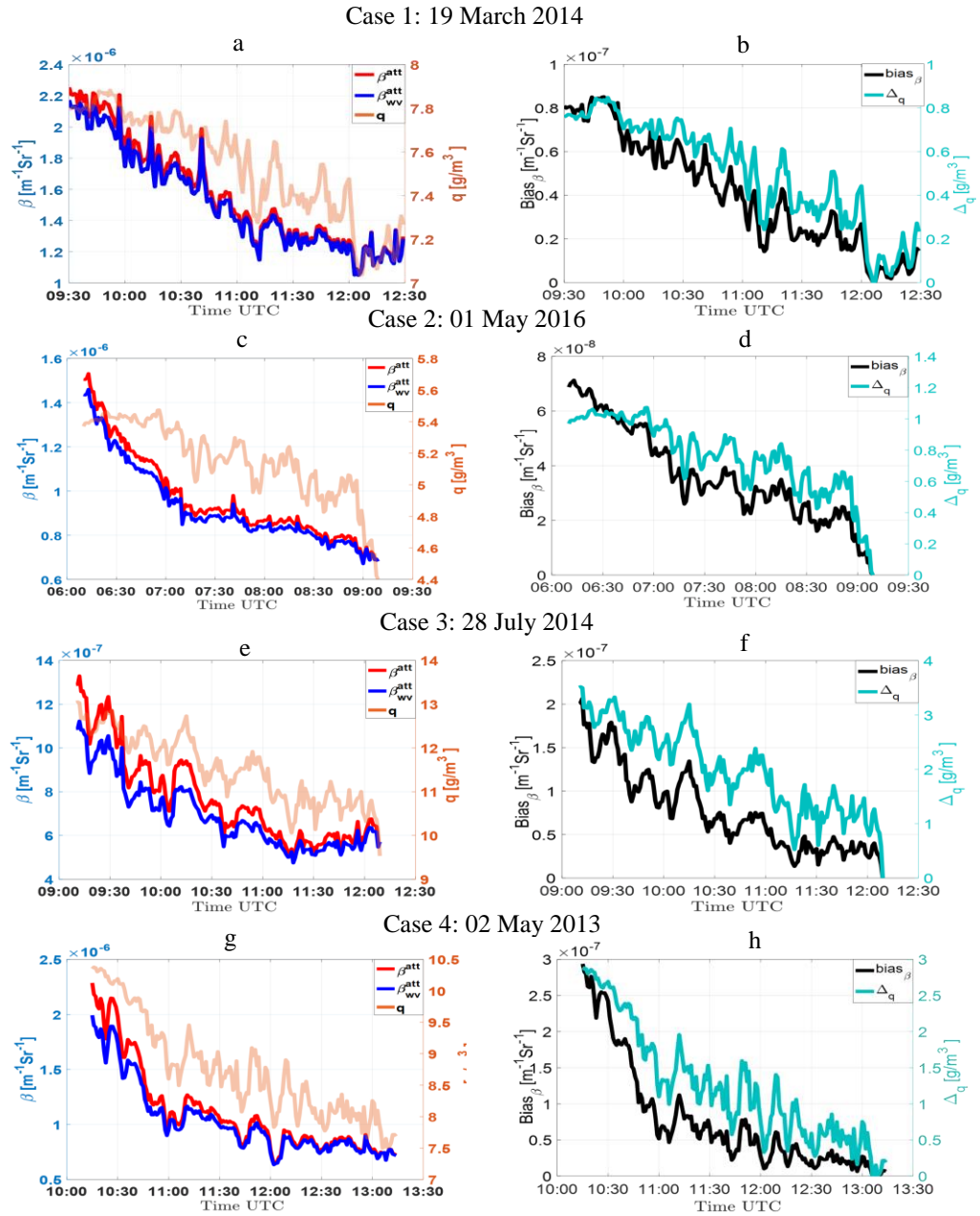


Figure S1. Time evolution of β^{att} (blue line), β_c^{att} (red line) and q (orange line) [left panels (a,c,e,g) bias_β (black line) and Δ_q (green line) [right panel (b,d,f,h)].

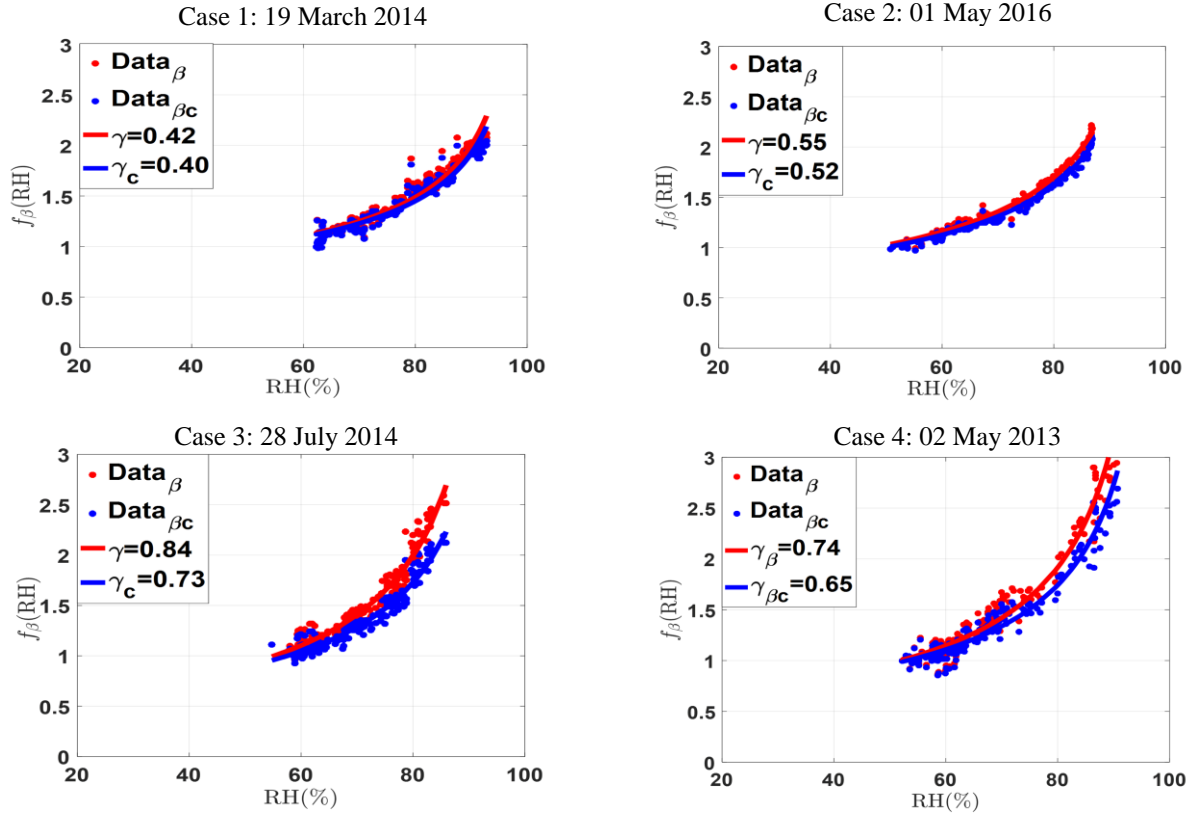


Figure S2. Experimental data points (blue/red dots) and Hänel parameterization (blue/red lines). Case 1 and Case 2 show the effect of the lower bias $_\beta$ and Δ_q differences over $f_{\beta_{wv}^{att}}(RH)$ and $f_\beta(RH)$. Case 3 and Case 4 present the effect of the higher bias $_\beta$ and Δ_q differences over $f_{\beta_{wv}^{att}}(RH)$ and $f_\beta(RH)$.

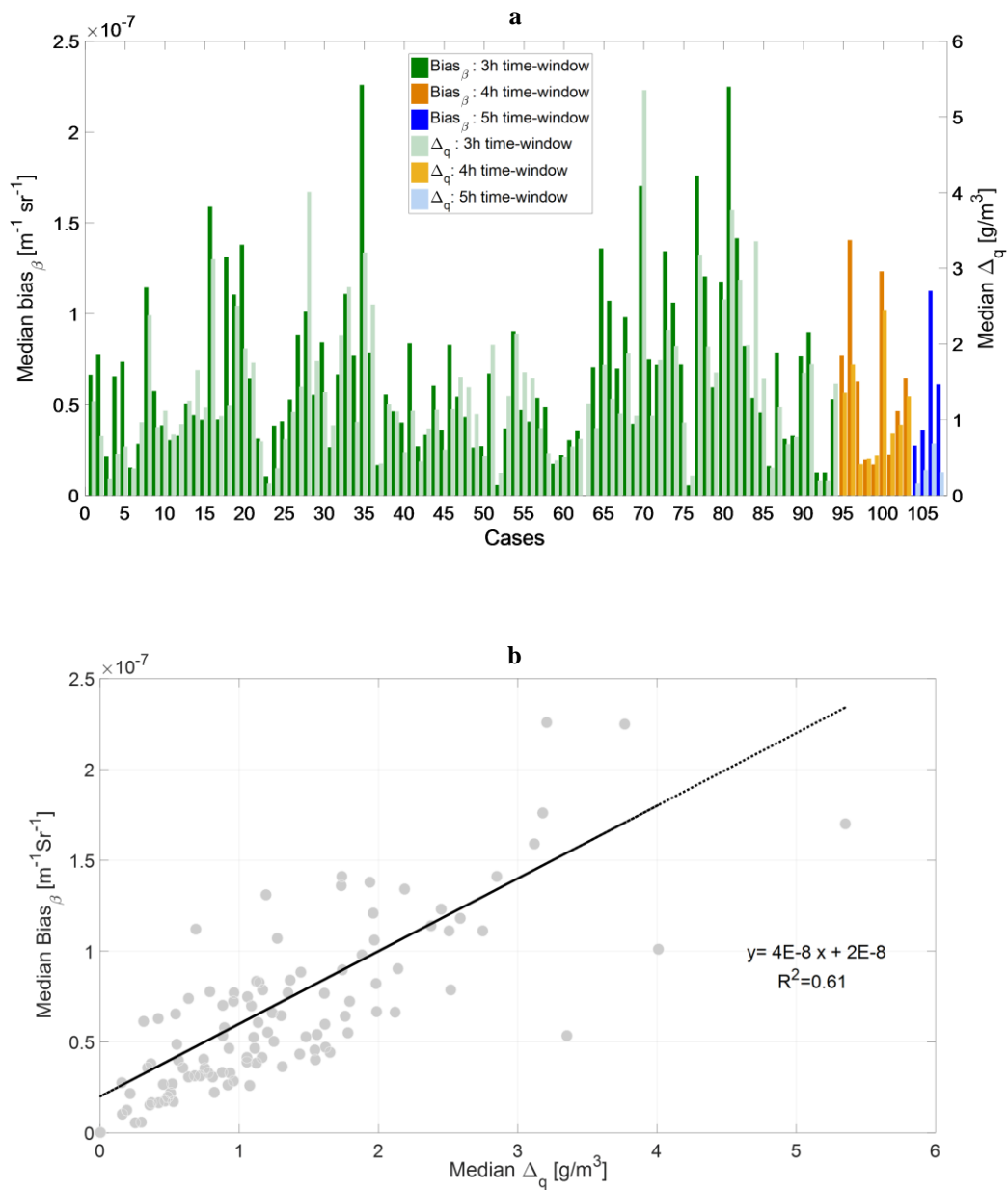


Figure S3. Median of bias_β and Δ_q for all potential cases of hygroscopic growth found from 2012 to 2016 at the ACTRS SIRTa observatory: (a) median of bias_β and Δ_q to 3h time-window analysis (green bars), 4h time-window analysis (orange bars) and 5h time-window analysis (blue bars); (b) scatter plot correlating median of bias_β and Δ_q for whole time-windows.

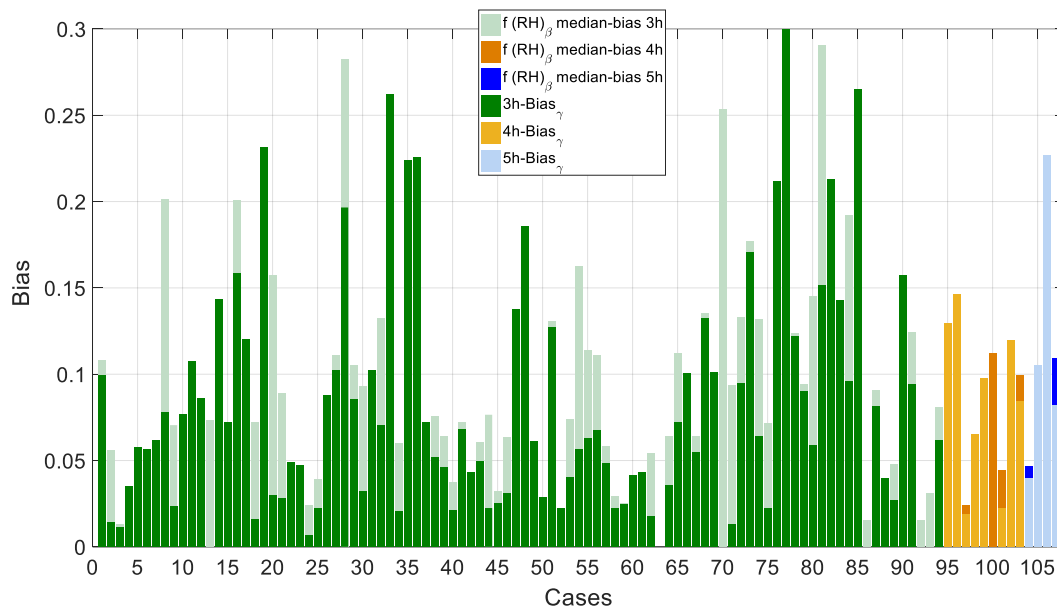


Figure S4. $\text{bias}_{f_{\beta}(RH)}$ and bias_{γ} for all potential cases of hygroscopic growth found from 2012 to 2016 at the ACTRIS SIRTA observatory. $\text{bias}_{f_{\beta}(RH)}$ and bias_{γ} for 3h time-window analysis (green bars), 4h time-window analysis (orange bars) and 5h time-window analysis (blue bars).

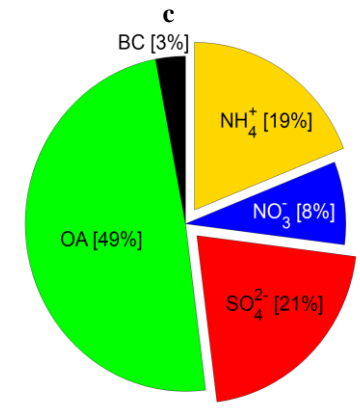
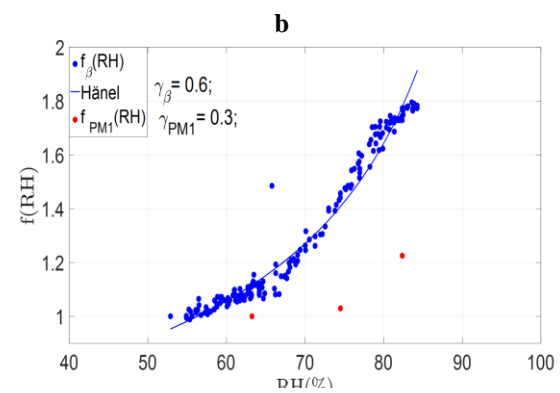
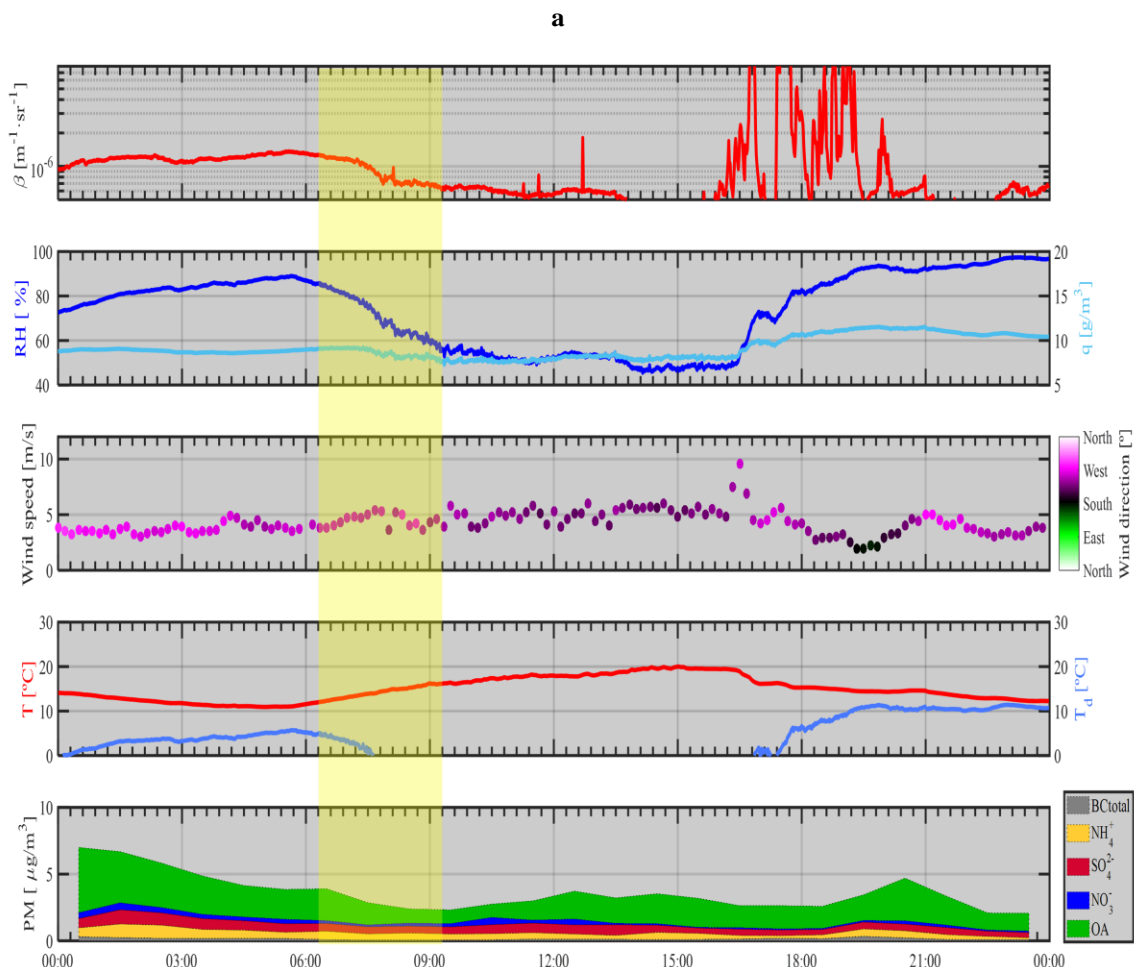


Figure S5. Criterion for data selection: case 1 on 29 July 2012 from 06:30 to 09:30 UTC.

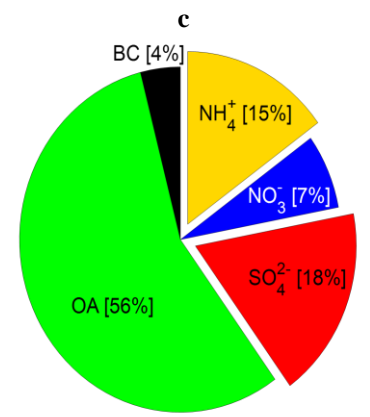
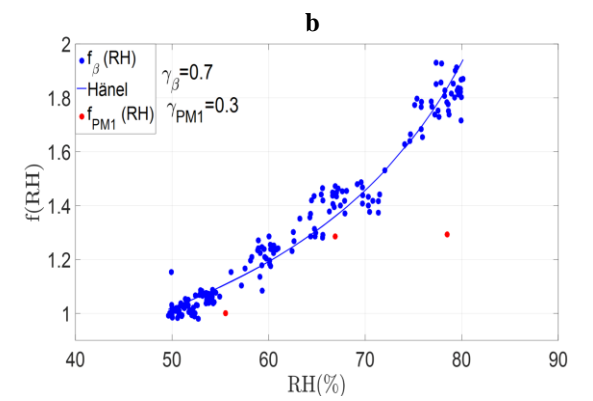
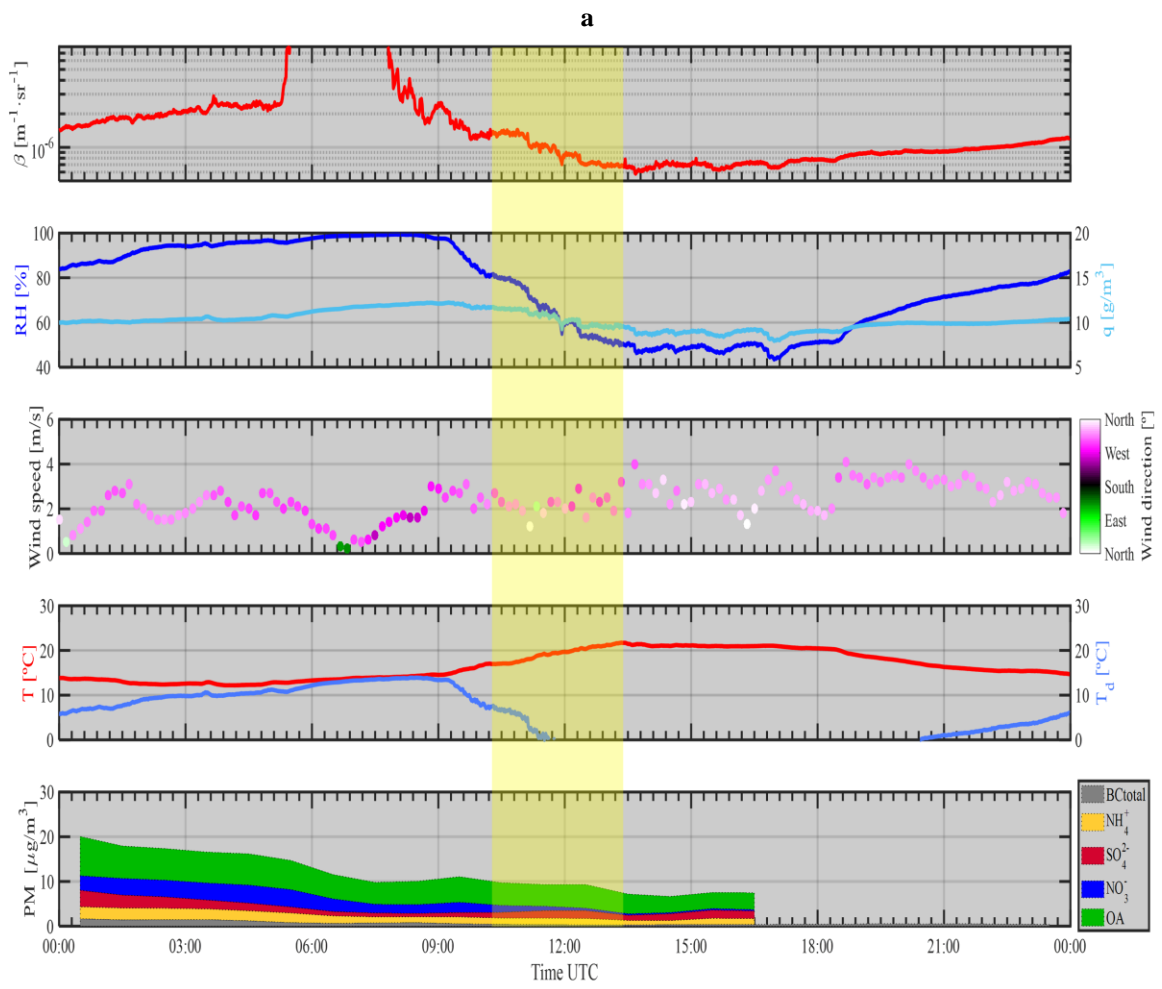


Figure S6. Criterion for data selection: case 2 on 02 September 2012 from 10:30 to 13:30 UTC.

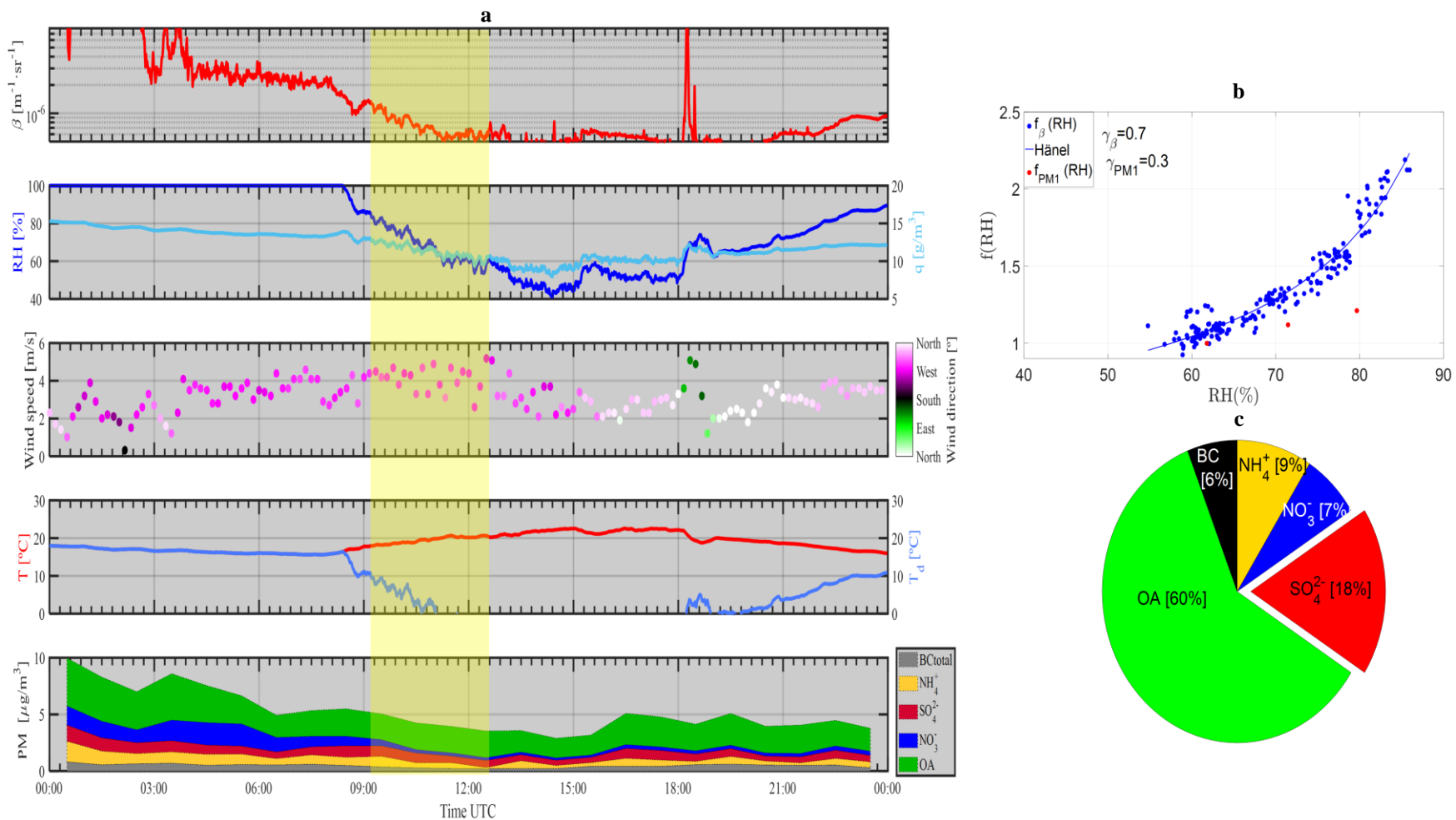


Figure S7. Criterion for data selection: case 4 on 28 July 2014 from 09:10 to 12:10 UTC.

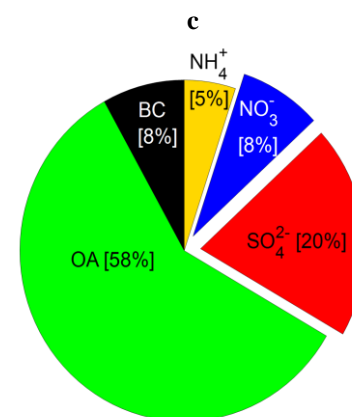
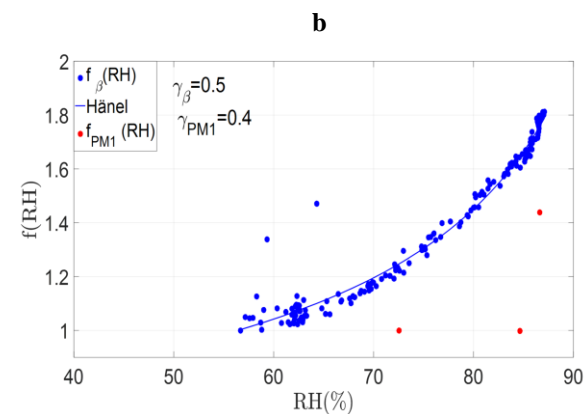
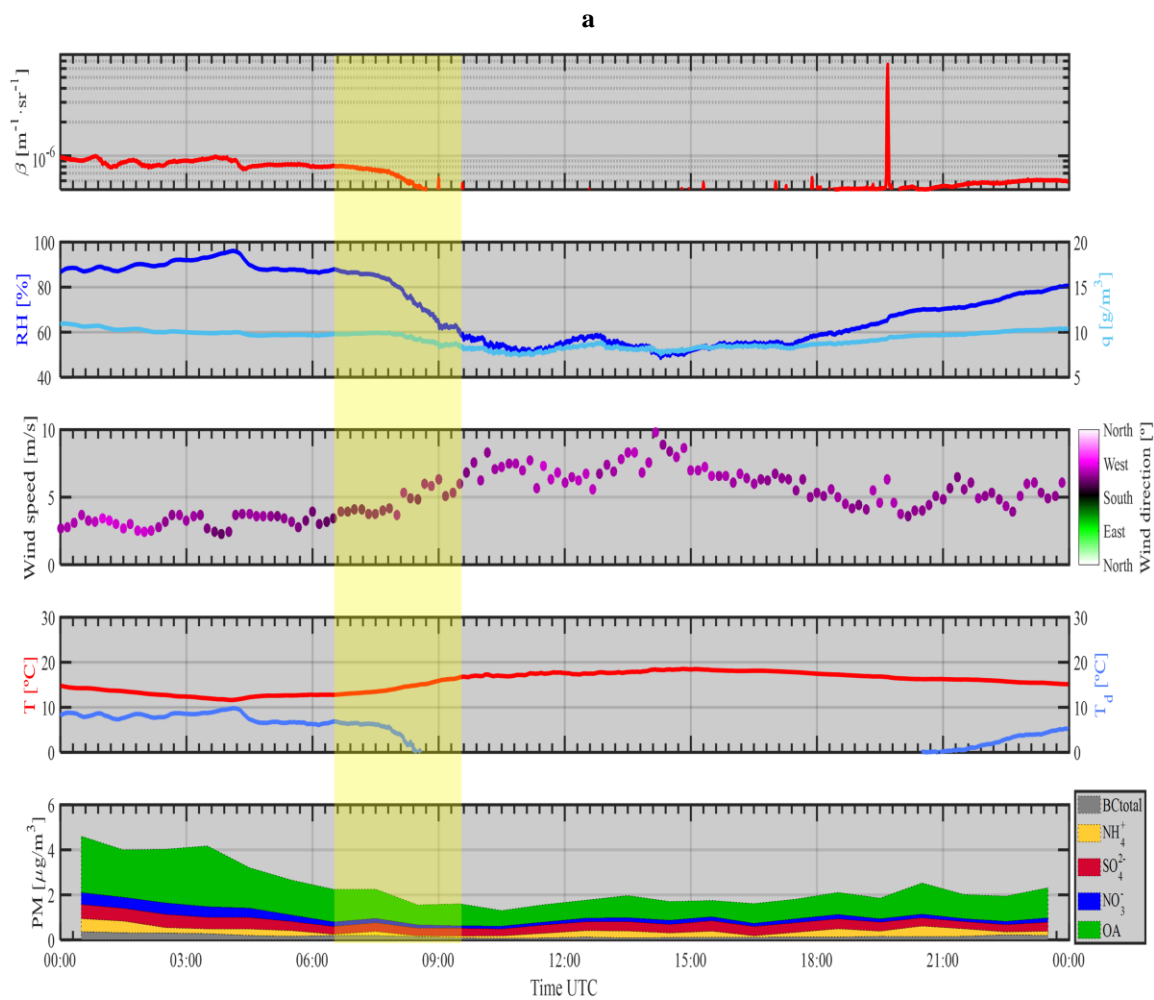


Figure S8. Criterion for data selection: case 5 on 17 August 2014 from 06:40 to 09:40 UTC.

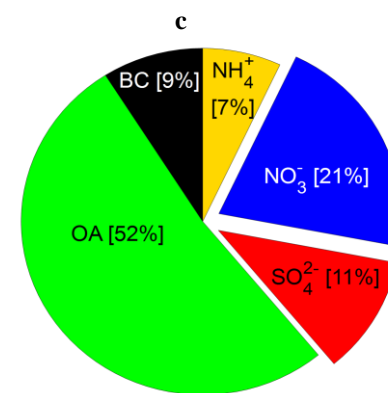
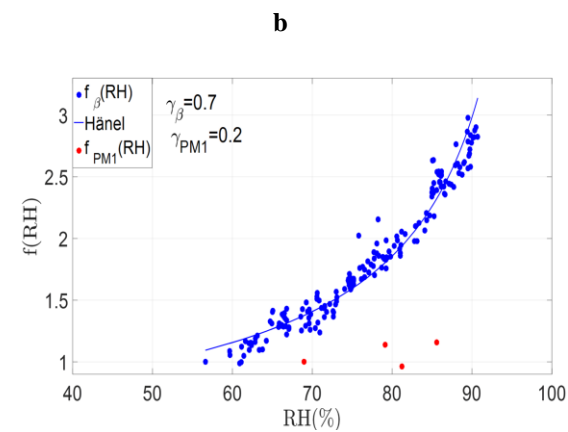
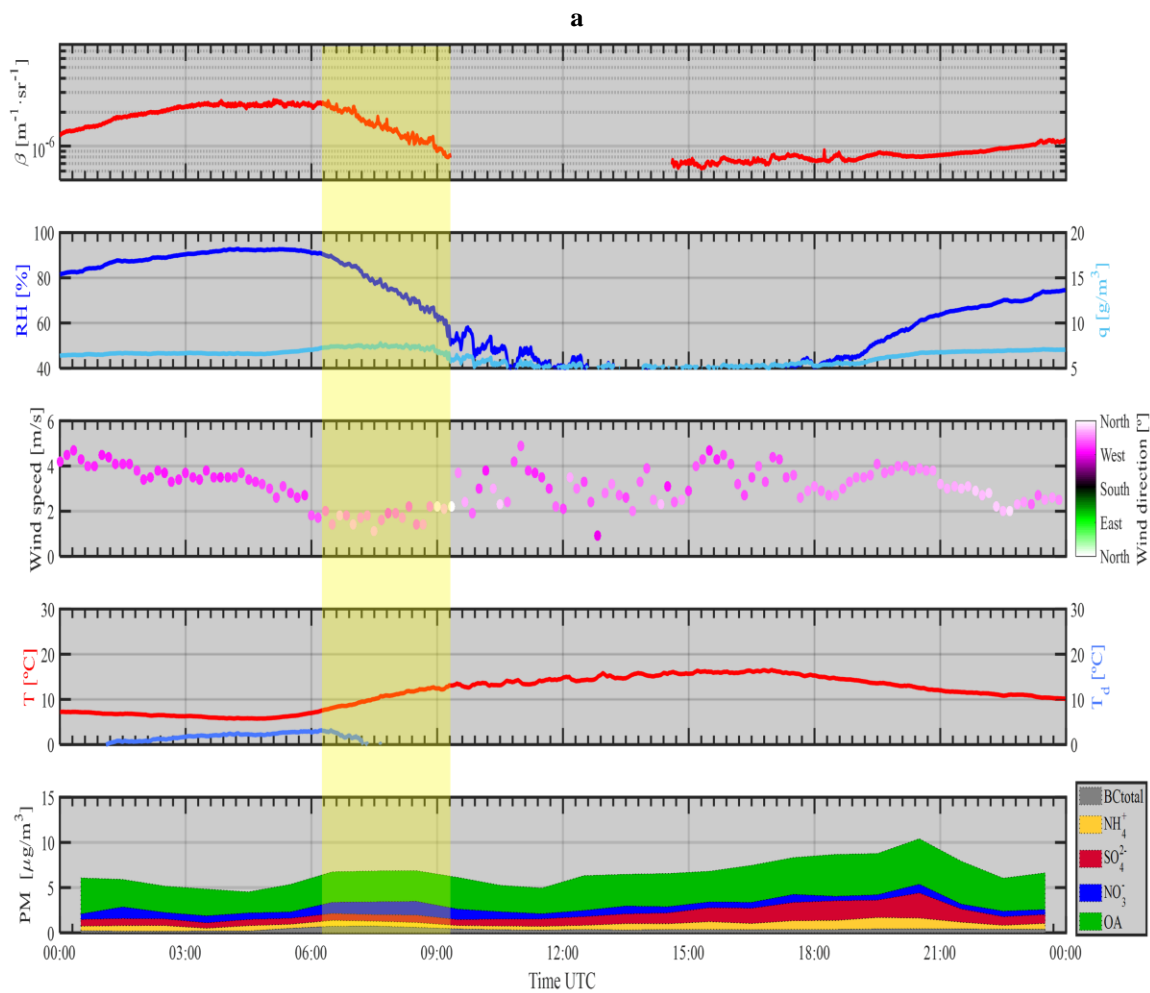


Figure S9. Criterion for data selection: case 6 on 21 May 2015 from 06:15 to 09:15 UTC.

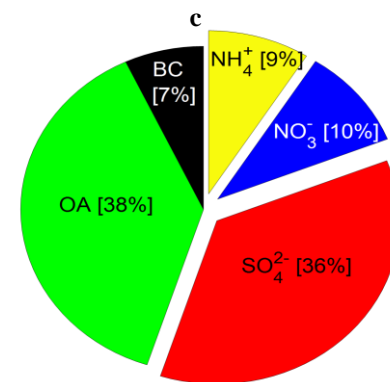
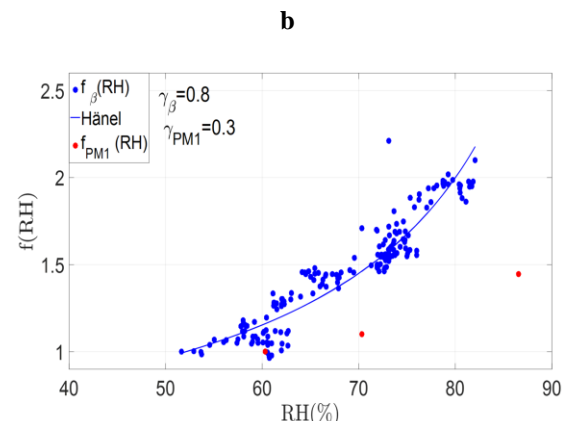
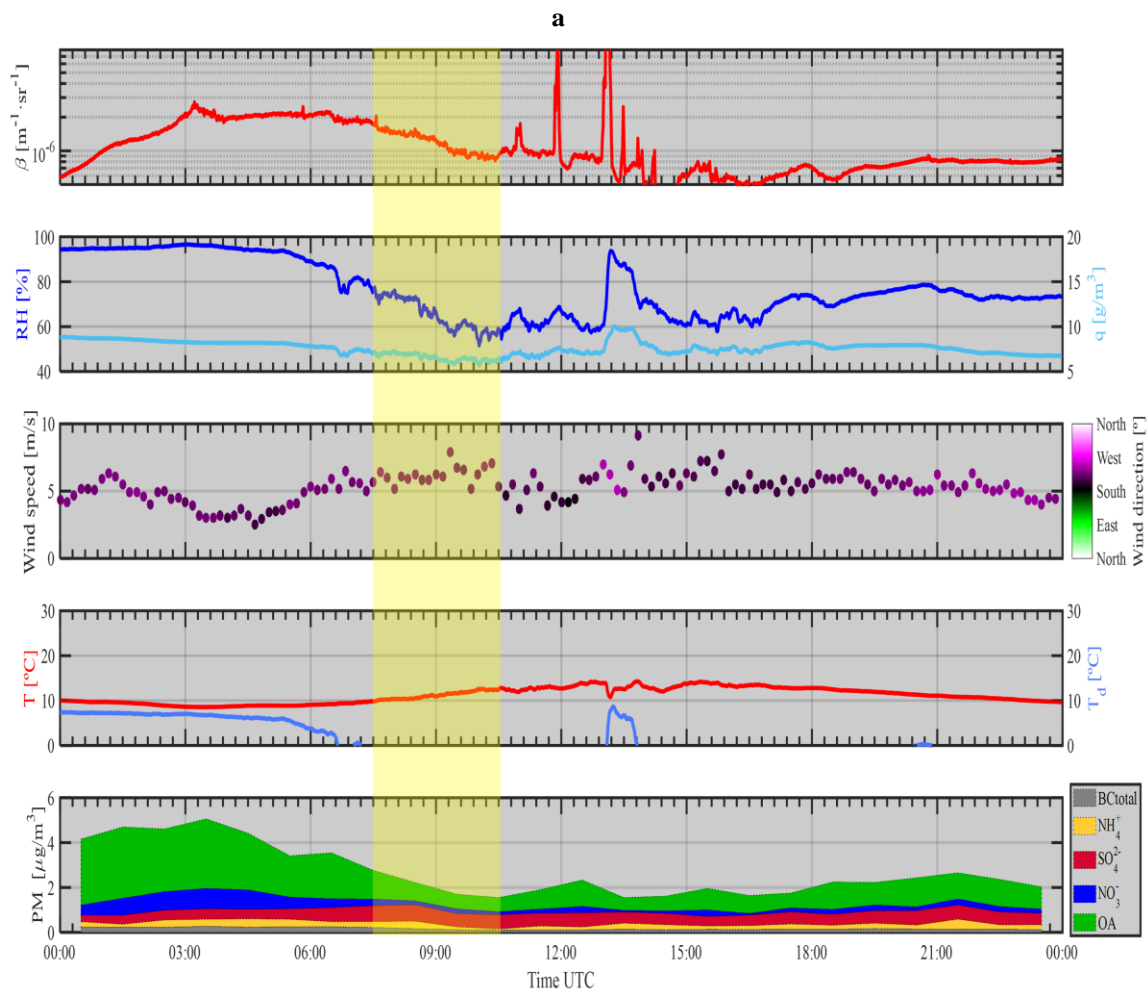


Figure S10. Criterion for data selection: case 7 on 15 April 2016 from 07:05 to 10:05 UTC.